HHS Public Access

Author manuscript

J Orthop Res. Author manuscript; available in PMC 2022 August 01.

Published in final edited form as:

J Orthop Res. 2021 August ; 39(8): 1811–1824. doi:10.1002/jor.24785.

Multiphasic scaffold for scapholunate interosseous ligament reconstruction: a study in the rabbit knee

Hayman Lui[1], **Cedryck Vaquette**[2,*], **Janet M. Denbeigh**[3,*], **Randip Bindra**[1,4], **Sanjeev Kakar**[3,†], **Andre J. van Wijnen**[3,†]

[1]Griffith University, School of Medicine, Gold Coast, Queensland, Australia

[2]The University of Queensland, School of Dentistry, Brisbane, Queensland, Australia

[3]Mayo Clinic, Department of Orthopedic Surgery, Rochester, Minnesota, United States of America

[4]Gold Coast University Hospital, Department of Orthopaedic Surgery, Gold Coast, Queensland, Australia

Abstract

Scapholunate interosseous ligament tears are a common wrist injury in young and active patients that can lead to suboptimal outcomes after repair. This research aims to assess a multiphasic scaffold using 3D-printing for reconstruction of the dorsal scapholunate interosseous ligament. The scaffold was surgically implanted in vivo in the position of the native rabbit medial collateral ligament. Two branches of treatment were implemented in the study. In the first group, the rabbits (n=8) had the knee joint fixed in flexion for 4 weeks using 1.4mm K-wires prior to sample harvesting. The second group (n=8) had the rabbit knee joint immobilised for 4 weeks prior to K-wire removal and mobilisation for an additional 4 weeks prior to sample harvesting. Overall, samples were harvested at four week post-surgery (immobilised group) and eight weeks post-surgery (mobilised group). Mechanical tensile testing (n=5/group) and histology (n=3/group) of the constructs were conducted. Tissue integration and maturation was observed resulting in increased mechanical strength of the operated joint at 8 weeks ($p<0.05$). Bone and ligament tissues were regenerated in their respective compartments with structural and mechanical properties approaching those reported for the human dorsal SLIL ligament.

Statement of Clinical Significance: This proof of concept study has demonstrated that the synthetic multiphasic scaffold was capable of regenerating both bone and ligament while also withstanding the physiological load once implanted in the rabbit knee. The artificial scaffold may provide an alternative to current techniques for reconstruction of scapholunate instability or other ligament injuries in the hand and wrist.

[†]**Corresponding AuthorsProf Andre van Wijnen,** Department of Orthopedic Surgery and Biochemistry & Molecular Biology, Mayo Clinic, Rochester, Minnesota, USA, +1-507-293-2105, vanWijnen.Andre@mayo.edu, **Dr Sanjeev Kakar,** Department of Orthopedic Surgery, Mayo Clinic, Rochester, Minnesota, USA, kakar.sanjeev@mayo.edu.

[*]denotes authors contributed equally

Author Contributions Statement

Hayman Lui contributed to all stages of the project including: research design, surgical procedure, data collection, analysis and drafting of the final manuscript. Cedryck Vaquette contributed to research design, data analysis/ interpretation and drafting of the final manuscript. Janet Denbeigh contributed to ethics preparation, research design, surgical procedure and data collection. Randip Bindra contributed to research design and design of the surgical procedure. Senior authors Andre van Wijnen and Sanjeev Kakar contributed to research design, data interpretation and manuscript drafting. All authors have read and approved the final submitted manuscript.

Keywords

3D-printing; tissue-engineering; ligament reconstruction; hand surgery

Introduction

The scapholunate interosseous ligament (SLIL) is a C-shaped ligament located in the wrist between the scaphoid and lunate bones[1]. It is particularly important for carpal stability during movements such as the dart throwing motion[2]. With perpendicular collagen fibres inserting in the scaphoid and lunate, the dorsal region is considered to be an important contributor to the ligament's biomechanical strength[3, 4].

SLIL injuries are common in young and active individuals with chronic tears often resulting in carpal instability, potentially leading to arthritis and loss of function[5]. Hence, SLIL injuries represent a significant health burden and decrease in life quality. Current surgical approaches are focused on the reconstruction of the dorsal region due to its biochemical importance. However, these surgical treatments primarily attempt to restore the biomechanical function of the ligament without necessarily allowing tissue regeneration, leading to suboptimal outcomes.

Given the limitations in current surgical techniques, a new strategy for SLIL reconstruction utilising the principles of tissue engineering enabling both mechanical stabilisation and tissue regeneration in a porous biomaterial structure is sound. Our group has previously reported the development of an additively manufactured multiphasic construct for the reconstruction of the dorsal segment of the SLIL along with the scaffold's biomechanical and biological properties[6]. This report established the proof of concept that a 3D-printed medical polycaprolactone (mPCL) construct with distinct architectural features in the ligament and bone compartments while maintaining a porous interface that could be manufactured in a continuous manner for utilisation in SLIL regeneration. This previous study demonstrated that the combination of the cell sheet technology in the ligament compartment along with the delivery of osteogenic cues (in the form of bone morphogenetic protein-2 encapsulated in a hydrogel) resulted in spatially confined and compartmentalised bone and ligament-like tissue formation, while enabling interaction of these tissues at the interface. Furthermore, the mPCL did not impact on the cell viability of human bone marrow mesenchymal stem cells during in vitro culture[6].

We have previously assessed the ability of our scaffold to maintain its compartmentalisation properties in an ectopic rodent model. However, it is necessary to test the scaffold compartmentalisation properties in a more physiologically and biomechanically relevant model. Therefore, this present study reports on the testing of the multiphasic scaffold in a rabbit model designed to recapitulate the anatomical features of the human dorsal SLIL. This was achieved by implanting the multiphasic scaffold in the knee at the location of the medial collateral ligament (MCL) and assessing the biological in vivo response in a biomechanically functioning joint.

Methodology

Scaffold Manufacturing and Characterisation

Multiphasic scaffold manufacturing—The methods of manufacturing have been described previously[6]. Briefly, a continuous printing process resulted in fabrication of connected fibres forming a construction with 0/90° orientation between layers (in the bone compartment) and a 0/0° arrangement in the ligament compartment (aligned fibres) with a layer thickness of 300μm. The individual scaffolds had an elongated U-shape whereby the bone compartments had a dimension of $5\times5\times10mm^3$ and were bridged by the ligament compartment with dimensions of 10mm length, 5mm width and 3mm height as shown in Figure 1.

SEM—The multiphasic scaffolds (n=3) were mounted on aluminium stubs, and sputter-coated for 150 seconds using gold-palladium. Samples were imaged in a Hitachi S-4700 cold field emission scanning electron microscope at 5kV accelerating voltage.

In Vivo Implantation

Multiphasic scaffold preparation—16 scaffolds (8 per group) were used for in vivo implantation. Firstly, scaffolds were etched by immersion in 5M NaOH at 37°C for 30 minutes before being washed three times (5-minute duration) with distilled H_2O. This was performed to increase the scaffold hydrophilicity. Secondly, the scaffolds were incubated in 100% ethanol at room temperature for 30 minutes before being sterilised under UV light for 30 minutes. This sterilisation protocol is well established and has been previously described in the literature [6–8].

Animal model and care—7-month old male New Zealand white rabbits (n=16) from Covance were acclimatised for 14 days and deemed to be of suitable health by a veterinarian before undergoing surgery. The rabbits were randomly allocated to either treatment (scaffold implantation with mobilisation post K-wire removal) or control group (scaffold implantation with no mobilisation). The multiphasic scaffold was implanted into the rabbit knee and the postoperative course of all animals was uneventful. The samples were retrieved at 4 weeks (while the knee joint was immobilised) or at 8 weeks (where the k-wire was removed enabling mobilisation of the knee joint for an additional 4 weeks). The level of bone formation and connective alignment were characterised in the corresponding compartments at 4 and 8 weeks. All experiments received Mayo Clinic Ethics Approval (IACUC Protocol A00002704–17) and experimentation was adherent to the code for the care and use of animals for scientific purposes.

Surgical technique for in vivo scaffold placement—Anaesthesia was performed using intramuscular injection of ketamine and isofluorane inhalation. The rabbit were placed in lateral position and knee in full flexion, the medial aspect of the left knee joint was carefully shaved, prepared and draped in sterile manner. A superficial longitudinal incision was made (in line with the patella position) to reflect the skin and expose the knee joint. The retinaculum was then incised, blunt dissected from the underlying muscle and reflected. Figure 2A-C illustrates the process of inserting the 1.6mm Kirshner wires

(K-wires) longitudinally from mid-shin on the tibia through to the femur to secure the knee joint in full flexion. The native MCL was exposed and the proximal end was excised from the medial tubercle of the femur (Figure 2D-F). A 5mm trephine burr and 5mm spherical burr was used to drill one central cavity for fitting the scaffold bone compartment in the femur medial tubercle at the site of MCL attachment (Figure 2G). A template scaffold was used to mark out the location of the distal bone trough (Figure 2H). A 5mm trephine burr and 5mm spherical burr were used to drill a central cavity in the tibia.

Next, a 1.8mm round burr and 4mm oval burr were used to widen the bone troughs superficially and to shave down bone adjacent to the knee joint in order to fit the scaffold (Figure 2I). Elevators were used to protect the menisci of the knee joint during this process. It was ensured that the alignment of the scaffold was the same as that of the native MCL. In vivo constructs were implanted into the knee joint by press-fitting the bone compartments into the drilled cavities (Figure 2J & P). Holes with a diameter of 0.7mm and 10mm depth were drilled for staple placement (Figure 2K). Two 8mm staples (positioned across each bone compartment) were hammered into the drilled holes to fix the scaffold to the femur and tibia (Figure 2L, M & P).

The retinaculum and skin were individually closed over to cover the scaffold and sutured with 4–0 vicryl monofilament (Figure 2N & O). Surgical area was washed with saline and swabbed with betadine to disinfect the wound. An x-ray was taken using a mobile C-arm machine to confirm adequate placement of K-wire and staples (Figure 2Q).

K-wire removal—At 4 weeks post-implantation, the animals were anesthetised and the surgical site was shaved and the underlying skin was disinfected using betadine antiseptic. A 1cm incision was made over the femoral end of the K-wire. The K-wire was cut and removed using pliers. The incision was sutured using 4.0 vicryl monofilament sutures and an x-ray was taken of the leg (Figure 2R).

Animal sacrifice and sample harvesting—The animals were euthanised by intravenous injection of pentobarbital sodium (150mg/kg of Lethabarb, 25G needle) at the 4 (n=8) & 8 (n=8) week time point. K-wires were removed from remaining samples. The knee joint containing the scaffold was extracted (Figure 3A-D) and fixed in 4% paraformaldehyde for 7 days before being placed in PBS for subsequent analysis. The samples were divided between histology (n=3 for each group at each time point and native MCL) and biomechanical testing (n=5 for each group at each time point).

MicroCT—Samples were analysed by microCT (μCT40, SCANCO Medical AG, Brüttisellen, Switzerland) with a voltage of 55kVp, a current of 145μA and power of 8W, an integration time of 300ms and a voxel size of 30μm to qualitatively evaluate bone mineralisation. 3D images were reconstructed using the microCT software.

Histology—In order to enable paraffin and hard tissue sectioning, the retrieved specimens (implanted and healthy knee joints, Figure 3A-D) were resected *en bloc* using a 0.4mm diamond blade saw (Figure 3E). The samples were thereafter longitudinally sectioned and

one section further processed for paraffin embedding while the remaining portion was processed for hard tissue histology.

Hematoxylin and eosin (H&E) staining—The staples were gently removed from the tissue and the samples were decalcified using 5M EDTA at room temperature for 3 weeks prior to dehydration and paraffin embedding using a tissue processor (Shandon™ Excelsior ES, Thermo Scientific, Waltham, USA). 5μm thick longitudinal slices of the constructs were sectioned and were stained with H&E.

Goldner's trichrome staining—The samples were dehydrated in a graded series of ethanol and resin infiltrated (MethylMethacrylate/Glycol Methacrylate, Tecknovit 7200, Heraeus Kulzer, Germany). Once cured, resin blocks were sectioned and lapped to a final thickness range of 30–50μm. The thin specimens were then stained with Goldner's trichrome stain.

Histomorphometry—Histomorphometry was conducted using the ImageScope suite. The surface area occupied by bone mineralisation, early stages of mineralisation (as defined by condensation of cell in a dense collagen matrix) and fibre alignment in the ligament compartment were measured in order to quantify the performance of the multiphasic scaffold.

Biomechanical testing

Tensile testing was performed on twenty samples in total from four different groups: 4 week in vivo multiphasic scaffold (n=5) (4 weeks), 8 week in vivo multiphasic scaffold (n=5) (8 weeks) and for comparison purposes on native rabbit MCL (n=5) (Native MCL), and multiphasic scaffold implanted ex vivo (n=5) (Ex Vivo). Ex vivo implantation was conducted in order to accurately test the biomechanical strength of the multiphasic construct in vivo. This was done on cadaveric rabbit knees (n=5) of the same age and similar knee joint dimensions as the animals used for in vivo experimentation.

The connective tissue over the region of the native MCL/scaffold/repair site was removed and the joint capsule, lateral collateral ligament, anterior cruciate ligament and posterior cruciate ligament were sectioned under loupe magnification. The rabbit tibia and femur were potted in 2.5cm diameter tubes using bone cement such that the knee joint and the knee ligament attachment sites were not contacting the bone cement. The length, width, and thickness of the native MCL/Scaffold/Repair site were measured with a digital caliper (Digimatic Absolute, Mitutoyo, Aurora, IL). The peak load and displacement of the scaffold were quantified. The scaffold stiffness was calculated from the slope of the linear region of the load-strain curve.

Using digital image correlation (DIC), live strain mapping during tensile testing was conducted. The native MCL/Scaffold/Repair site was prepared following similar techniques previously published in the literature[9, 10]. We followed the recommendations of the International Digital Image Correlation Society as closely as possible, having a speckle pattern on the site's medial surface with each speckle being 3–5 pixels in diameter, as close

to 50/50 distribution of black and white on the specimen as feasible, and creating facets with 3–5 speckles per facet.

Samples were then mounted to a servo-hydraulic test machine (model 858, MTS, Minneapolis, MN) using a custom fixture. Each specimen was preloaded at 0–3% strain prior to being loaded in tension to failure under displacement control at a rate of 20mm/min. The DIC system (GOM 4M, Trillion Quality Systems, King Prussia, PA) consisted of two cameras with data collected at 32Hz used to analyse the surface strain and deformation response. The mapped component was Longitudinal Strain or the strain parallel to the loading direction. This was computed as technical/engineering strain (Δl/l0) as a tensile test had been conducted on the scaffolds. During data processing, any regions of questionable strain outcomes were investigated further by measuring the strain of individual facets and confirming the individual facet strain aligned with that of the local surrounding area. Data was also further checked by applying a median spatial filter to reduce any outliers.

Statistics

Sample Size Calculations—Power calculations were performed to determine the approximate sample size required to achieve 5% statistical significance. For histological assessments, we anticipated a 30% difference between groups, with a sample standard deviation of 12.5. To achieve a power of 0.8, we would require 3 animals in each treatment group for histology. For biomechanical assessments, we anticipated a 30% difference between groups, with a sample standard deviation of 15 to account for variability in the mounting of tissues on the biomechanical strain tester. To achieve a power of 0.8, we would require 4 animals in each treatment group. For this study, 5 animals per treatment group were used to account for any potential early losses. Therefore, a total of 16 rabbits with 8 animals per group were used in these experiments.

Statistical Significance—One-way ANOVA with a Tukey post-hoc for multiple comparisons was used for determining statistical significance in histomorphometry and biomechanical tensile tests as more than two means were compared (IBM SPSS Statistics for Windows version 21.0, IBM Corporation 2012©, Armonk, NY, USA). A $p \leq 0.05$ was considered to represent statistically significant differences.

Results

Scaffold Morphology

SEM visualisation of the scaffold in Figure 1 illustrates a modified version of the multiphasic scaffold designed and reported in our previous study[11]. The length of the ligament compartment measured 10mm to more accurately mimic the size of the multiphasic scaffold that would potentially be used for human implantation. Indeed, current clinical practices involve the placement of the bone anchor several millimetres from the ligament attachment sites in the scaphoid and lunate bones in order to prevent bone fractures. The average strut diameter was 410±18μm (n=5) and there was some fusion at the strut contact points of the alternating layers similarly to our previous report[6].

In Vivo Characterisation

Micro-computed tomography and histology—Bone formation was qualitatively assessed using microCT and this demonstrated the maintenance of the tissue compartmentalisation as no heterotopic ossification was observed in the intra-articular space. Specifically, bone formation was restricted to the bone compartment and followed the scaffold architecture (Figure 4A). At 8 weeks, significantly more bone mineralisation was observed compared to the 4-week samples as shown by micro-computed tomography (Figure 4B).

This was also confirmed using two different stainings; H&E (Figure 5) and Goldner's trichrome staining (Figure 6). At 4 weeks the bone compartments were fully infiltrated by the host tissue which consisted of interspersed fatty marrow (Figure 5 & 6) with the presence of occasional bone islets surrounding the PCL filament of the 3D-printed scaffold. The 8 week time point presented similar histological morphology although more bone was present (Figure 6B). This was confirmed by the histomorphometry demonstrating a significant increase in bone area (1.8 ± 0.3 mm^2 at 4 weeks compared to 6.5 ± 1.3 mm^2 at 8 weeks, $p<0.05$). Again, no heterotopic bone formation was present at this later time point which indicated that the multiphasic scaffold alone was capable of stimulating ossification that was restricted to the bone compartment only.

Ligament compartment—Histological analysis of the ligament compartment demonstrated dense, aligned fibres enriched with collagen without the presence of inflammatory cells at both 4 weeks and 8 weeks (Figure 5 & 6). Histomorphometry analysis demonstrated that the ligament compartment had significantly higher amounts of fibre alignment at 8 weeks (10.1 ± 2.4mm^2) when compared to 4 weeks (2.8 ± 1.3mm^2) and the native MCL (4.1 ± 0.5mm^2) (Figure 8D, $p<0.05$). This highlighted the fibre-guiding properties of the scaffold in forming new aligned ligamentous tissue bridging the bone compartments. In all samples, it was observed that the ligament fibres inserted into the bone compartment via the porous interface thereby regenerating the bone-ligament enthesis (Figure 7). This was confirmed in Goldner's trichrome stain (Figure 6) where a greater amount of soft tissue regeneration is seen at 8 weeks compared to 4 weeks (red and blue staining in ligament compartment). Overall, the scaffold was able to withstand physiological loading over 8 weeks in vivo (including a 4 week joint mobilisation) as no failure or filament fraying was observed in either the intra-articular or bone-ligament interface regions.

Biomechanical testing—All in vivo samples failed in the mid-section of the scaffold (Table 1). The strain maps in Figure 8A illustrate that the native MCL had strain distributed across a larger surface area of the tendon. This can be compared to the strain map of the rabbit knees containing scaffolds that showed a more localised strain pattern (Figure 8B&C). In addition, the failure point for the scaffold was within the ligament compartment. This suggests that while localised deformation of the scaffold is not ideal, the bone compartment was still well integrated within the resident bone preventing undesirable slipping and therefore acting as a strong anchor for the ligament. Overall, this indicates that the bone-ligament interface of the scaffold was strong enough to withstand the physiological force of the rabbit knee.

The primary benefit of live strain mapping technique was that it enabled local deformation behaviour to be identified. As the scaffold would have undergone changes due to tissue ingrowth during the 4 or 8 weeks in vivo, tensile testing along the axis of the ligament compartment explains the uneven strain concentrations observed.

The mechanical properties of the multiphasic scaffold were assessed by quasi-static tensile testing (Figure 9, Table 1). Ex vivo testing of the scaffold implanted in the cadaveric rabbit joint demonstrated that it had an ultimate force of 75 ± 9N. This was not significantly different from the ultimate force of the in vivo scaffold at 4 weeks, indicating that at this time point the scaffold was the main contributor of the biomechanical properties of the joint. After 8 weeks, however, the ultimate force increased significantly reaching 118 ± 18N, indicating that bone and ligament tissue regeneration and maturation had occurred and the newly formed tissue participated to withstanding the physiological load, leading to an increase in the biomechanical properties of joint. There was no significant difference in ultimate strain of the samples showing that the scaffold did not undergo extensive softening over the time course of the in vivo study. Despite the remodelling and maturation process in the multiphasic scaffold as seen in the histology, the stiffness of the Ex Vivo, 4 Week and 8 Week groups remained similar and no significant differences were observed. However, a significant difference in stiffness was observed between the Native MCL and the other groups as expected.

Discussion

This study developed an animal model for testing the regenerative and biomechanical properties of a multiphasic scaffold for application in dorsal scapholunate interosseous ligament reconstruction. To this end, a lapine MCL model was utilised due to the ethical concerns and limitations associated with the SLIL regenerative models in high primates. While the MCL rabbit model does not entirely recapitulate the biological and biomechanical features of the human SLIL, it represents a step forward into the assessment of SLIL implants in a more a more realistic biological environment and under dynamic biomechanical loading.

Numerous animal models have been developed for orthopaedic applications targeting ligament or tendon reconstruction. These include ectopic models[12, 13], rabbit ACL[14, 15] or flexor tendon models[16] and sheep ACL[17–19] or rotator cuff models[20]. The SLIL ligament is unique due to its specific anatomy and complex biomechanical loading which has not been recapitulated in these established models. Given its location in the wrist carpal bones and its importance in stabilising refined movements such as ‘dart-throwing’, the SLIL is only present in higher order animals such as primates. However, there have been no experimental studies conducted using a primate model due to ethical and financial concerns. As a result, there is no suitable animal model that allows for the simultaneous assessment of a scaffold’s biomechanical strength and regenerative capacity for SLIL reconstruction.

In fact, ex vivo studies on human cadaveric specimens are the current gold standard of the field for research in new SLIL grafts or surgical techniques prior to clinical implementation. They have been conducted extensively to characterise the biomechanical properties of

potential SLIL autografts from intrinsic hand ligaments as well as ligaments from the foot[21–24] or other synthetic structures[25]. While the use of cadaveric studies allows for tailoring of SLIL grafts to match the biomechanical strength of the native ligament, this does not account for the tissue regeneration or remodelling events occurring or for the biomechanical fatigue and biodegradation behaviour of the prosthesis.

Our previous research utilised a small animal model in order to establish a proof-of-concept in an ectopic site for tissue regeneration[6]. There were limitations inherent to this model as it failed to recapitulate the SLIL vascular or the biomechanical loading environment. Due to the dimensional restrictions encountered in mice or rats, the implantation of the multiphasic scaffold into the paws of these animals cannot be successfully performed. A rabbit model was selected for this study, in part because the rabbit femur and tibia have similar dimensions as the scaphoid and lunate bones[26]. Furthermore, the rabbit MCL width is of the same dimensions as that of the dorsal SLIL (around 5 mm length and 3–4 mm width). While extensive histological quantification of the rabbit MCL has demonstrated that it is hypovascular in this intra-articular region hence mirroring the native environment of the native SLIL[27], the vasculature of the bone structures greatly differ. Indeed, the tibial plateau and femoral head had a high degree of vascularisation, which is in contrast to scaphoid and lunate bones whereby the main vascular network is located further away from the ligament insertion sites. This can have important consequences on bone tissue regeneration in the multiphasic scaffold and therefore may not reflect the SLIL clinical situation.

This study aimed to test a multiphasic scaffold for possible SL reconstruction in humans. This involved the drilling of holes in the femur and tibia for the bone compartments and a press-fitted approach of implanting the scaffold with the use of titanium staples to secure the construct. Overall, the scaffold demonstrated extensive bone regeneration with no ectopic ossification indicating that the immobilisation period with K-wire fixation in knee flexion is essential to ensure sufficient stability of the bone plugs. This aligns with current SLIL reconstruction protocols in humans whereby the joint is also immobilised for a certain period allowing for the proper integration of the bone plugs prior to resuming movement and the transmission of the biomechanical forces.

A major limitation of this model was the different biomechanical loading, and consequently the mechanobiological signalling pattern of the rabbit knee joint when compared to a human wrist. The MCL is the primary stabiliser against valgus deformation to the knee and also prevents internal rotation and posterior tibia translation[28]. In contrast, the main biomechanical forces acting on the SLIL are in the torsional plane, with the ligament preventing excessive scaphoid flexion and lunate extension[4, 29]. Despite, the differential loading pattern, the human SLIL and the rabbit MCL display similar ultimate force of several hundredths of Newtons[29–33].

The success of the multiphasic graft characterised in this study can be judged by its biomechanical properties and histological features after implantation compared to the native SLIL ligament. Firstly, a key element of success for any graft used in SLIL reconstruction is in its ability to maintain the reduced SL joint over time. The force required for scapholunate joint reduction has been investigated extensively in the literature and ranges

from 20N-50N[34, 35]. A biomechanical study of the rabbit knee has shown that the load on the MCL ligament is between 10 and 20N during hopping[36]. Therefore the load experienced by the scaffold in the rabbit joint is on the lower range of the human SLIL physiological force[37, 38]. This indicates that tissue regeneration is required in order to withstand the physiological load. Our study has demonstrated that tissue maturation over the 8 week implantation timeframe translated to an increased ultimate load, suggesting a mechanical reinforcement induced by the newly formed tissue.

Secondly, the histology of the multiphasic construct after implantation in vivo also mimicked the architecture found in the native SLIL ligament. In particular, the architecture of the ligament compartment consisting in multiple grooves created by the mPCL filaments imparted tissue-guiding properties. This resulted in increased ligament alignment at 8 weeks compared to 4 weeks as we previously reported albeit in an ectopic rodent model and hence without any biomechanical loading[6]. While tissue alignment in the ligament compartment was similar to that seen in the native MCL[39], the mobilisation of the joint and hence the repetitive cyclic loading for 4 weeks resulted in further alignment of the tissues possibly in the direction of the physiological load. This is in accordance with previous in vitro[40] and in vivo studies[18, 41] demonstrating the formation of a directionally orientated cells and/or ligament-like tissue. Certainly, this is corroborated by H&E staining and histomorphometry which highlighted a higher degree of collagenic fibre alignment in samples from the later time point.

There was a strong bone-ligament interface as demonstrated by the large number of inserted fibres into the bone compartment thereby approaching the native insertion sites of the dorsal SLIL in the lunate and scaphoid bones. Previous studies have also attempted to recapitulate the bone-ligament interface and Ma et al.[18] successfully generated a bone-ligament-bone construct for ACL reconstruction using osteoblast and fibroblast cell sheets pinned together and allowed to fuse laterally before implantation in a sheep model. Nokakova et al.[20] has also explored this cell sheet technology for use in repairing rotator cuff tears in a sheep model. While histological analysis confirmed the regeneration of a bone-tendon enthesis, there was no significant increase in tensile strength of these bone-ligament-bone grafts after a six month recovery period compared to the traditional double row suture repair approach. Given that ligament reconstructions in animal studies as well as human surgeries often fail at the bone-ligament interface, the current data highlights the potential of this multiphasic scaffold in overcoming this issue with adequate in vivo biomechanical strength and tissue regeneration resembling the native dorsal SLIL.

Conclusion

This study reported on a multiphasic scaffold which demonstrated compartmentalised tissue regeneration, a strong bone-ligament interface and maintenance of structural integrity throughout in vivo implantation in the rabbit knee. This is one step closer to clinical translation, validating the utilisation of the multiphasic scaffold in a more biologically relevant and biomechanically dynamic environment. Nevertheless, further studies on surgical fixation of the graft in human cadaveric specimens and possibly in higher order animals will be required to assess the long-term behaviour of the construct.

Acknowledgements

The researchers would like to thank the significant contribution of Dr Nicolas Reina (Centre Hospitalier Universitaire de Toulouse) and Dr Chenghao Zhang (Mckay Orthopedic Research Lab, University of Pennsylvania) who assisted in the surgical procedures of this study. Furthermore, we would like to thank the support of the Mayo Clinic Orthopedic Department Biomechanics Lab in addition to the Queensland University of Technology Histology Lab for assisting in relevant data analysis. This research was funded by an internal Mayo Clinic grant 'AR049069 to AJvW'. The authors have no conflicts of interest or financial disclosures in relation to this study.

References

1. Berger RA. The gross and histologic anatomy of the scapholunate interosseous ligament. J. Hand Surg. Am. 1996;21:170–178. [PubMed: 8683042]
2. Crisco JJ, Coburn JC, Moore DC, Akelman E, Weiss AP, Wolfe SW. In vivo radiocarpal kinematics and the dart thrower's motion. J. Bone Joint Surg. Am. 2005;87:2729–2740. [PubMed: 16322624]
3. Berger RA. The anatomy of the ligaments of the wrist and distal radioulnar joints. Clin. Orthop. Relat. Res. 2001:32–40. [PubMed: 11210966]
4. Berger RA, Imeada T, Berglund L, An KN. Constraint and material properties of the subregions of the scapholunate interosseous ligament. J. Hand Surg. Am. 1999;24:953–962. [PubMed: 10509273]
5. Kitay A, Wolfe SW. Scapholunate instability: current concepts in diagnosis and management. J. Hand Surg. Am. 2012;37:2175–2196. [PubMed: 23021178]
6. Lui H, Bindra R, Baldwin J, Ivanovski S, Vaquette C. Additively Manufactured Multiphasic Bone–Ligament–Bone Scaffold for Scapholunate Interosseous Ligament Reconstruction. Advanced healthcare materials. 2019;0:1900133.
7. Berner A, Reichert JC, Woodruff MA, et al.Autologous vs. allogenic mesenchymal progenitor cells for the reconstruction of critical sized segmental tibial bone defects in aged sheep. Acta biomaterialia. 2013;9:7874–7884. [PubMed: 23628773]
8. Sudheesh Kumar PT, Hashimi S, Saifzadeh S, Ivanovski S, Vaquette C. Additively manufactured biphasic construct loaded with BMP-2 for vertical bone regeneration: A pilot study in rabbit. Mater. Sci. Eng. C Mater. Biol. Appl. 2018;92:554–564. [PubMed: 30184782]
9. Naghibi H, Mazzoli V, Gijsbertse K, et al.A noninvasive MRI based approach to estimate the mechanical properties of human knee ligaments. Journal of the mechanical behavior of biomedical materials. 2019;93:43–51. [PubMed: 30769233]
10. Xu D, Wang Y, Jiang C, et al.Strain Distribution in the Anterior Inferior Tibiofibular Ligament, Posterior Inferior Tibiofibular Ligament, and Interosseous Membrane Using Digital Image Correlation. Foot Ankle Int. 2018;39:618–628. [PubMed: 29533732]
11. Lui H, Vaquette C, Bindra R. Tissue Engineering in Hand Surgery: A Technology Update. J Hand Surg Am. 2017;42:727–735. [PubMed: 28751113]
12. Kim YT, Park JC, Choi SH, et al.The dynamic healing profile of human periodontal ligament stem cells: histological and immunohistochemical analysis using an ectopic transplantation model. Journal of periodontal research. 2012;47:514–524. [PubMed: 22308979]
13. Vaquette C, Sudheesh Kumar PT, Petcu EB, Ivanovski S. Combining electrospinning and cell sheet technology for the development of a multiscale tissue engineered ligament construct (TELC). J. Biomed. Mater. Res. B Appl. Biomater. 2018;106:399–409. [PubMed: 28170157]
14. Ge Z, Goh JC, Lee EH. The effects of bone marrow-derived mesenchymal stem cells and fascia wrap application to anterior cruciate ligament tissue engineering. Cell transplantation. 2005;14:763–773. [PubMed: 16454351]
15. Ouyang HW, Goh JC, Lee EH. Use of bone marrow stromal cells for tendon graft-to-bone healing: histological and immunohistochemical studies in a rabbit model. The American journal of sports medicine. 2004;32:321–327. [PubMed: 14977654]
16. He M, Gan AW, Lim AY, Goh JC, Hui JH, Chong AK. Bone Marrow Derived Mesenchymal Stem Cell Augmentation of Rabbit Flexor Tendon Healing. Hand surgery : an international journal devoted to hand and upper limb surgery and related research : journal of the Asia-Pacific Federation of Societies for Surgery of the Hand. 2015;20:421–429.

17. Mahalingam V, Wojtys EM, Wellik DM, Arruda EM, Larkin LM. Fresh and frozen tissue-engineered three-dimensional bone-ligament-bone constructs for sheep anterior cruciate ligament repair following a 2-year implantation. Biores. Open Access. 2016;5:289–298.
18. Ma J, Smietana MJ, Kostrominova TY, Wojtys EM, Larkin LM, Arruda EM. Three-dimensional engineered bone-ligament-bone constructs for anterior cruciate ligament replacement. Tissue engineering. Part A. 2012;18:103–116. [PubMed: 21902608]
19. Teuschl AH, Tangl S, Heimel P, et al.Osteointegration of a Novel Silk Fiber-Based ACL Scaffold by Formation of a Ligament-Bone Interface. The American journal of sports medicine. 2019:363546518818792.
20. Novakova SS, Mahalingam VD, Florida SE, et al.Tissue-engineered tendon constructs for rotator cuff repair in sheep. J. Orthop. Res. 2018;36:289–299. [PubMed: 28657154]
21. Harvey EJ, Hanel D, Knight JB, Tencer AF. Autograft replacements for the scapholunate ligament: a biomechanical comparison of hand-based autografts. J Hand Surg Am. 1999;24:963–967. [PubMed: 10509274]
22. Cuenod P, Charriere E, Papaloizos MY. A mechanical comparison of bone-ligament-bone autografts from the wrist for replacement of the scapholunate ligament. J. Hand Surg. Am. 2002;27:985–990. [PubMed: 12457348]
23. Svoboda S, Eglseder W, Belkoff S. Autografts from the foot for reconstruction of the scapholunate interossesous ligament. J. Hand Surg. Am. 1995;20:980–985. [PubMed: 8583071]
24. Davis CA, Culp RW, Hume EL, Osterman AL. Reconstruction of the scapholunate ligament in a cadaver model using a bone-ligament-bone autograft from the foot. J. Hand Surg. Am. 1998;23:884–892. [PubMed: 9763267]
25. Eng K, Wagels M, Tham SK. Cadaveric scapholunate reconstruction using the ligament augmentation and reconstruction system. J Wrist Surg. 2014;3:192–197. [PubMed: 25097813]
26. Crum JA, LaPrade RF, Wentorf FA. The anatomy of the posterolateral aspect of the rabbit knee. Journal of orthopaedic research : official publication of the Orthopaedic Research Society. 2003;21:723–729. [PubMed: 12798074]
27. Bray RC, Rangayyan RM, Frank CB. Normal and healing ligament vascularity: a quantitative histological assessment in the adult rabbit medial collateral ligament. J. Anat. 1996;188 (Pt 1):87–95. [PubMed: 8655419]
28. Amis AA, Robinson JR. The anatomy and biomechanics of the medial collateral ligament and posteromedial corner of the knee. The Knee Joint: Surgical Techniques and Strategies. Paris: Springer Paris; 2012:23–30.
29. Rajan P, Day C. Scapholunate interosseous ligament anatomy and biomechanics. J. Hand Surg. Am. 2015;40:1692–1702. [PubMed: 26143029]
30. Bray RC, Shrive NG, Frank CB, Chimich DD. The early effects of joint immobilization on medial collateral ligament healing in an ACL-deficient knee: A gross anatomic and biomechanical investigation in the adult rabbit model. Journal of Orthopaedic Research. 1992;10:157–166. [PubMed: 1740733]
31. Frank C, Woo SL-Y, Amiel D, Harwood F, Gomez M, Akeson W. Medial collateral ligament healing:A multidisciplinary assessment in rabbits. The American journal of sports medicine. 1983;11:379–389. [PubMed: 6650715]
32. Johnston JD, Small CF, Bouxsein ML, Pichora DR. Mechanical properties of the scapholunate ligament correlate with bone mineral density measurements of the hand. J. Orthop. Res. 2004;22:867–871. [PubMed: 15183447]
33. Nikolopoulos FV, Poulilios AD, Stamou AC, Papagelopoulos PJ, Zoubos AV, Kefalas VA. A simple constitutive model for the Scapholunate ligament. Medical Engineering & Physics. 2012;34:1196–1199. [PubMed: 22901856]
34. Dimitris C, Werner FW, Joyce DA, Harley BJ. Force in the Scapholunate Interosseous Ligament During Active Wrist Motion. J. Hand Surg. Am. 2015;40:1525–1533. [PubMed: 26026356]
35. Yi R, Werner FW, Sikerwar S, Harley BJ. Force Required to Maintain Reduction of a Preexisting Scapholunate Dissociation. J. Hand Surg. Am. 2018;43:812–818. [PubMed: 30049432]

36. Spelier EL, Shrive NG, Frank CB. Correlating rabbit movement with load on its medial collateral ligament. American Society of Mechanical Engineers, Bioengineering Division (Publication) BED. 1996;33:97–98.

37. King GJ, Damson EL, Frank CB, Shrive NG. A new device and method for controlling the load in rabbit medial collateral ligament reconstructions. J. Biomech. Eng. 1995;117:41–47. [PubMed: 7609483]

38. Thornton GM, Shrive NG, Frank CB. Healing ligaments have decreased cyclic modulus compared to normal ligaments and immobilization further compromises healing ligament response to cyclic loading. J. Orthop. Res. 2003;21:716–722. [PubMed: 12798073]

39. Anderson DR, Weiss JA, Takai S, Ohland KJ, Woo SL. Healing of the medial collateral ligament following a triad injury: a biomechanical and histological study of the knee in rabbits. J. Orthop. Res. 1992;10:485–495. [PubMed: 1613624]

40. Wang JHC, Yang G, Li Z, Shen W. Fibroblast responses to cyclic mechanical stretching depend on cell orientation to the stretching direction. Journal of Biomechanics. 2004;37:573–576. [PubMed: 14996570]

41. Florida SE, VanDusen KW, Mahalingam VD, et al.In vivo structural and cellular remodeling of engineered bone-ligament-bone constructs used for anterior cruciate ligament reconstruction in sheep. Connect. Tissue Res. 2016:1–13.

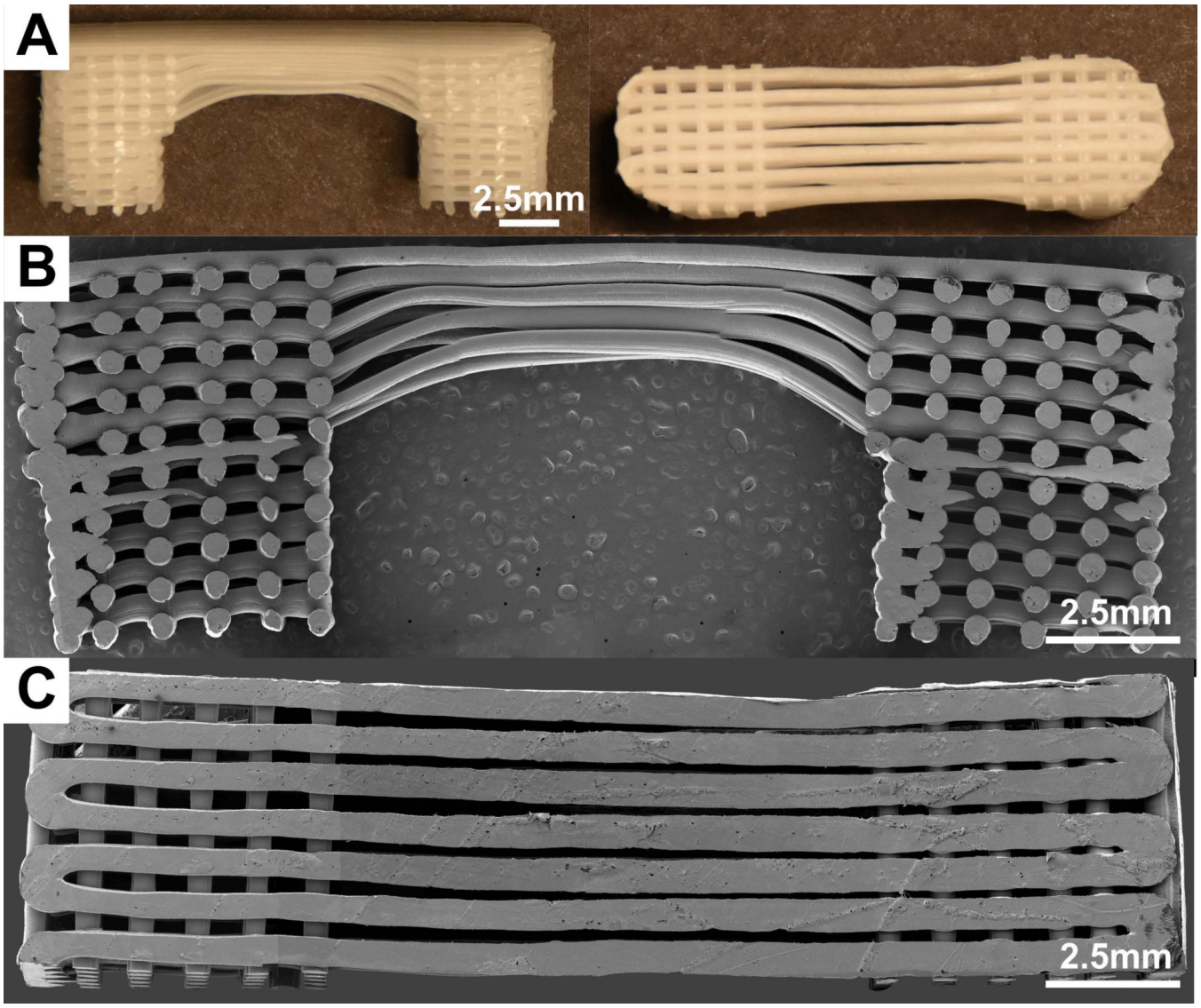

Figure 1:

Multiphasic scaffold used in rabbit implantation. **A)** Photographs of the scaffold with round bone compartments. **B-C)** Cross-section and top view of the multiphasic scaffold as seen by SEM.

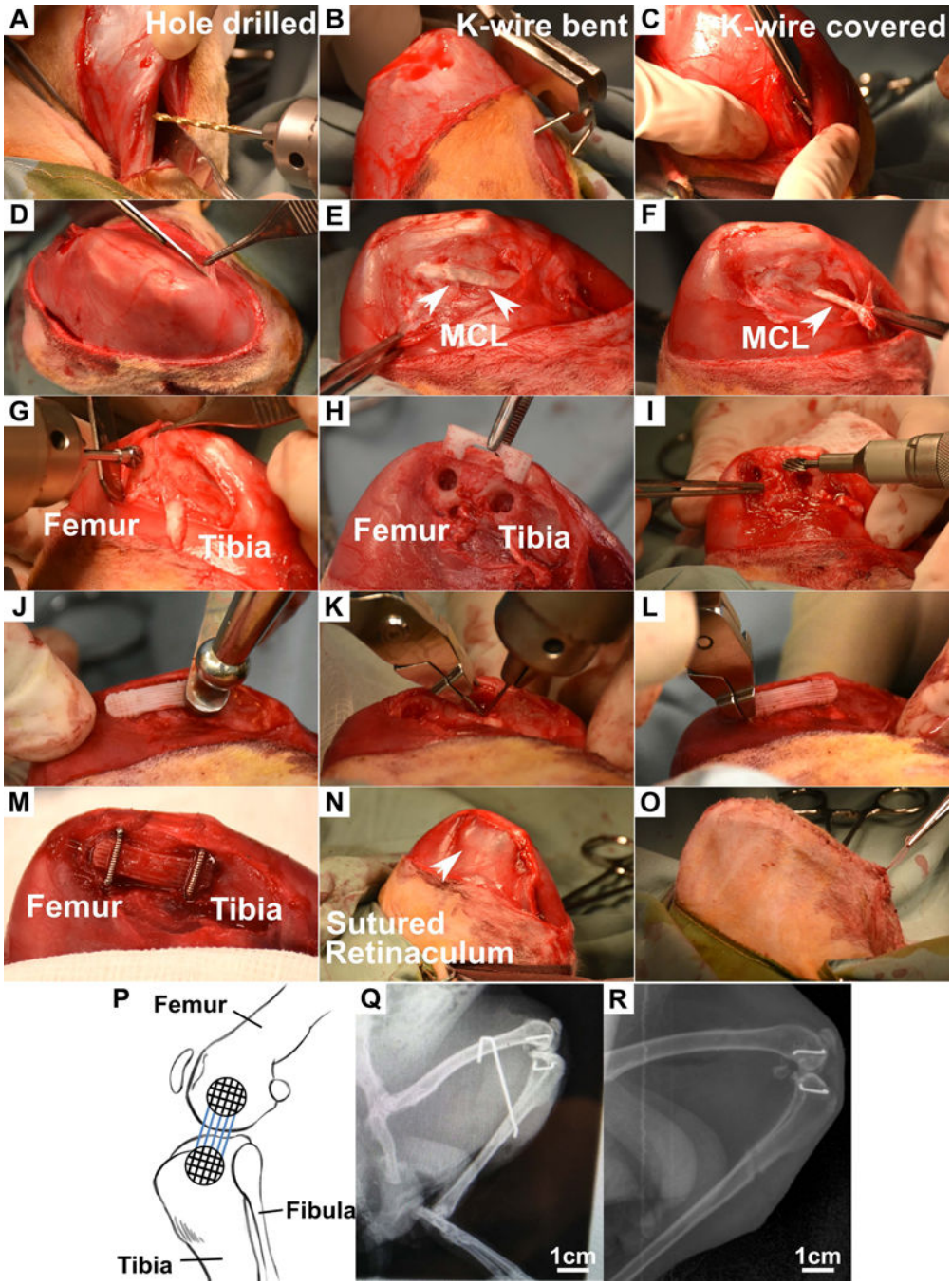

Figure 2:

Surgical procedure for implantation of the multiphasic scaffold into rabbit knee. **A)** A 1.6mm drill bit was used to drill longitudinally into the tibia and femur. **B)** The K wire was inserted through the drilled tunnel from the femur and bent to hook over the femur. **C)** The K-wire was bent on the tibial side and then cut short. **D)** Exposure of MCL in the medial side of the knee joint of the rabbit. **E)** Excision of the MCL from the medial tubercle on the femur. **G-H)** A 5mm trephine burr and 5mm spherical burr attached to a Stryker ¼" drill was used to drill a central cavity on the femur and tibia using a template scaffold as a

guide. **I)** 1.8mm round burrs and 4mm oval burrs were used to widen the bone troughs. **J)** Scaffold was press-fitted into bony cavities in the femur and tibia. K-**K-M)** 0.7mm diameter stables were inserted over the femur and tibia to hold the scaffold in place. **N-O)** The retinaculum and skin were sutured to close the wound. **P)** Stylistic diagram of a rabbit knee joint showing position of scaffold implanted **Q)** X-ray of rabbit leg post-implantation with K-wire holding the leg in flexion. Staples are seen on the medial side of the knee indicating the position of the scaffold. **R)** X-ray of leg after removal of K-wires. Line across the tibia indicates the position of the interosseous tunnel drilled for K-wire placement.

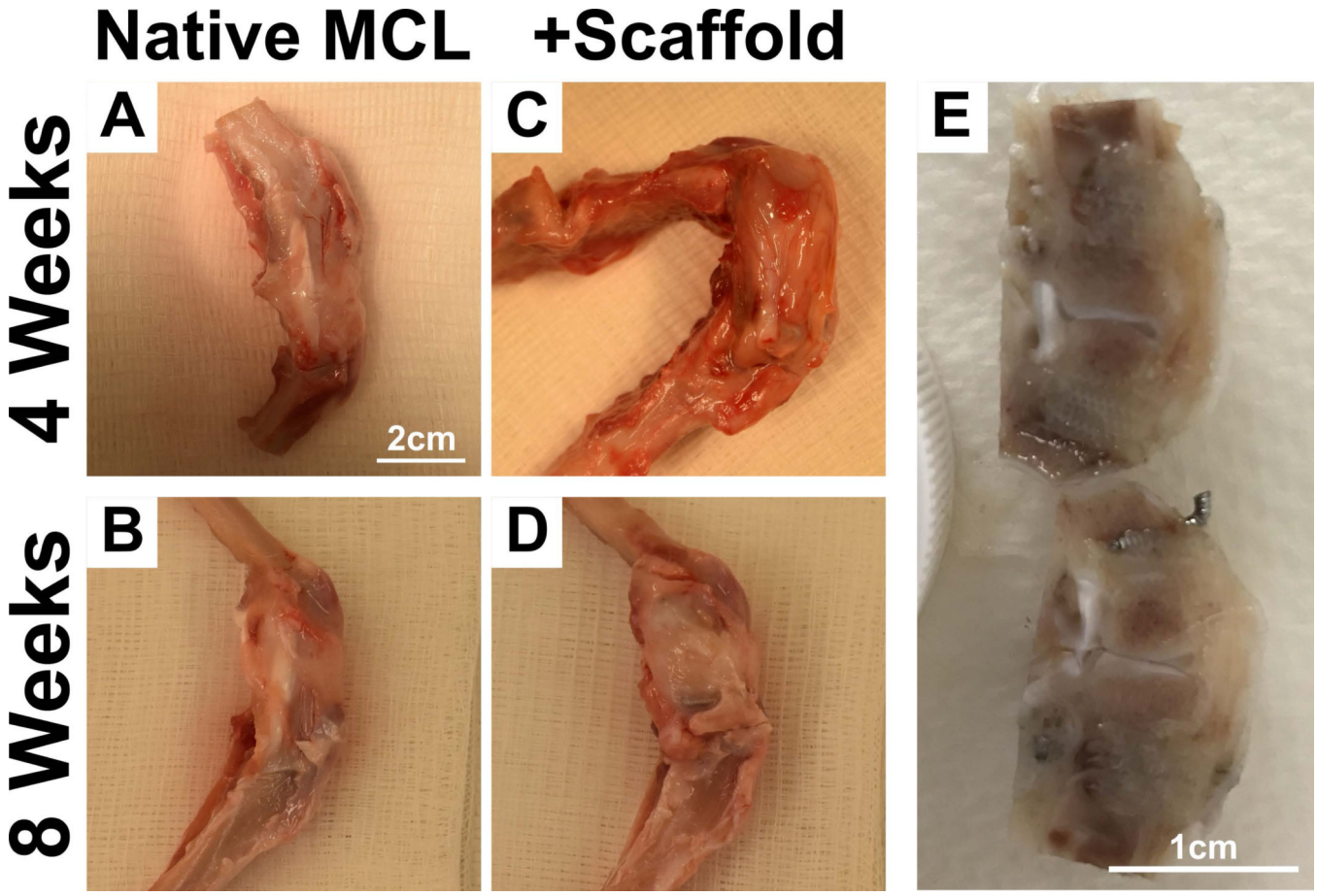

Figure 3:
Sample harvest from rabbits at 4 weeks and 8 weeks post-implantation. **A-D)** Native MCL and multiphasic scaffolds in the rabbit knee. **E)** Trimming of samples to isolate the scaffold prior to tissue processing for paraffin or resin embedding.

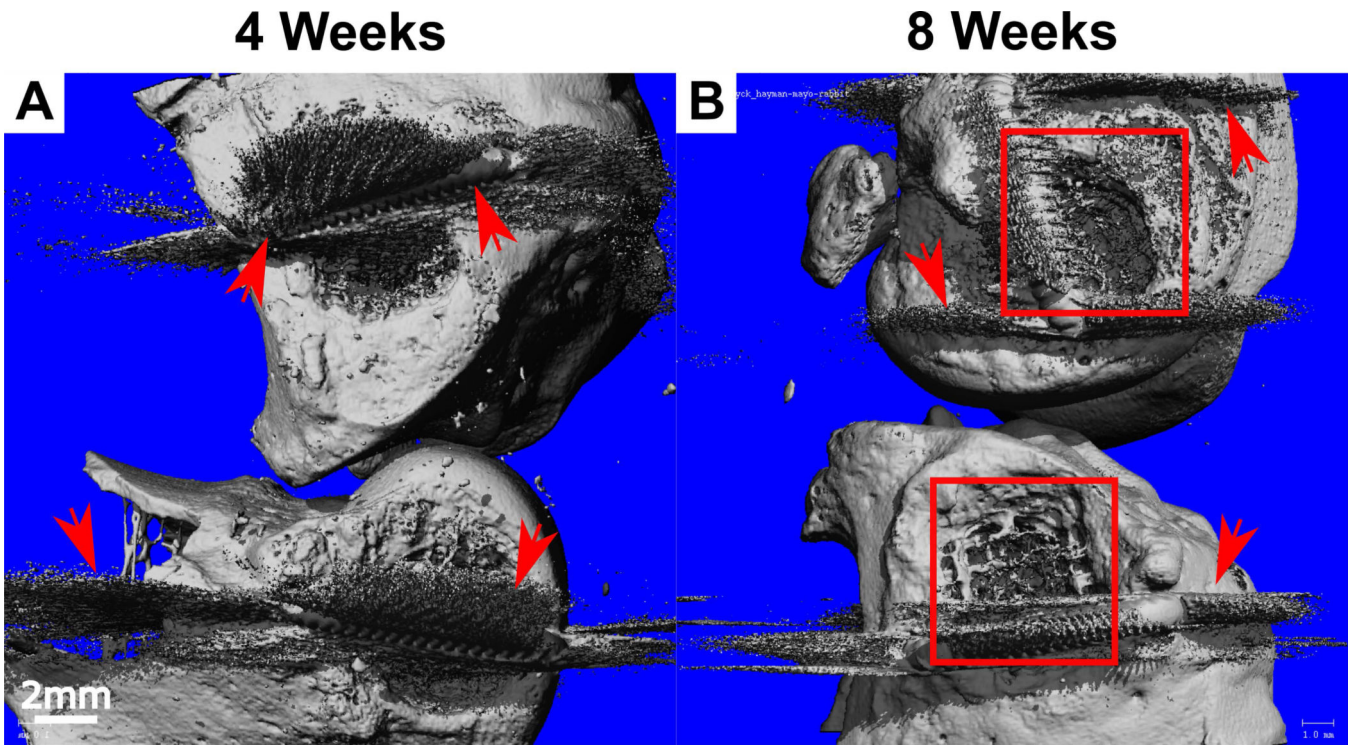

Figure 4:

MicroCT analysis of bone mineralisation at **A)** 4 weeks and **B)** 8 weeks post-implantation with the view from the medial aspect of the rabbit knee. Bone plugs with visible bone formation can be seen at 8 weeks (boxed). Arrows indicate the presence of scattering from the titanium staples.

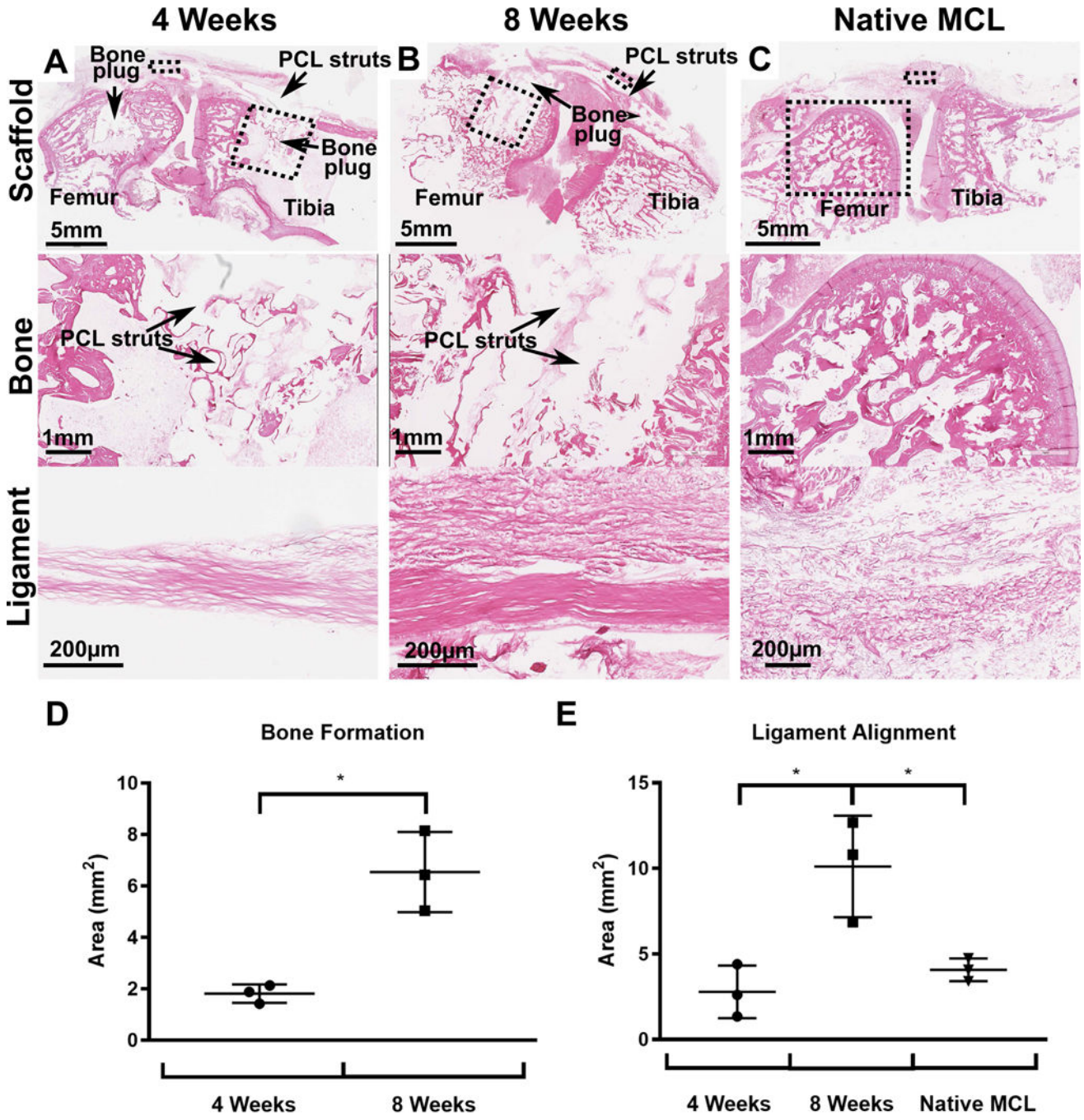

Figure 5:

Histological analysis of samples stained with H&E 4 weeks and 8 weeks post-implantation compared to native MCL. **A-C)** H&E staining of multiphasic constructs and native MCL. The dashed boxes refers to the region of scaffold under increased magnification in the images below. **D-E)** Histomorphometry analysis of bone formation and ligament alignment in the scaffolds and in native MCL.

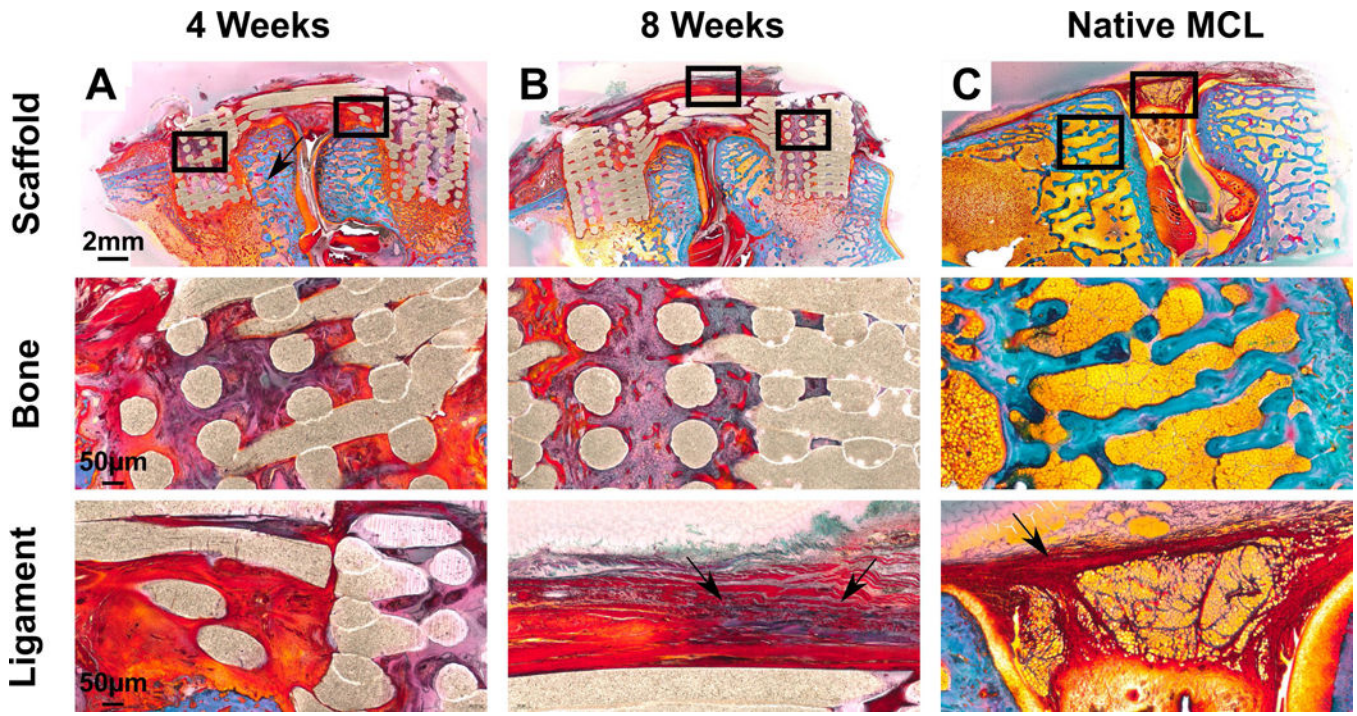

Figure 6:

Goldner's trichrome staining on resin embedded samples. Bone tissue is located here as shown by '*' and ligament tissue is visible running in parallel articulation to joint. Blue indicates collagen and red indicates the presence of connective tissue. The PCL scaffold used in the experiment is porous meaning that a void exists between two contact points. **A-B)** Scaffold in vivo at 4 weeks and 8 weeks. Greater soft tissue regeneration is seen at 8 weeks (red) with greater collagen staining (arrows) in the ligament compartment. **C)** Native rabbit MCL for comparison.

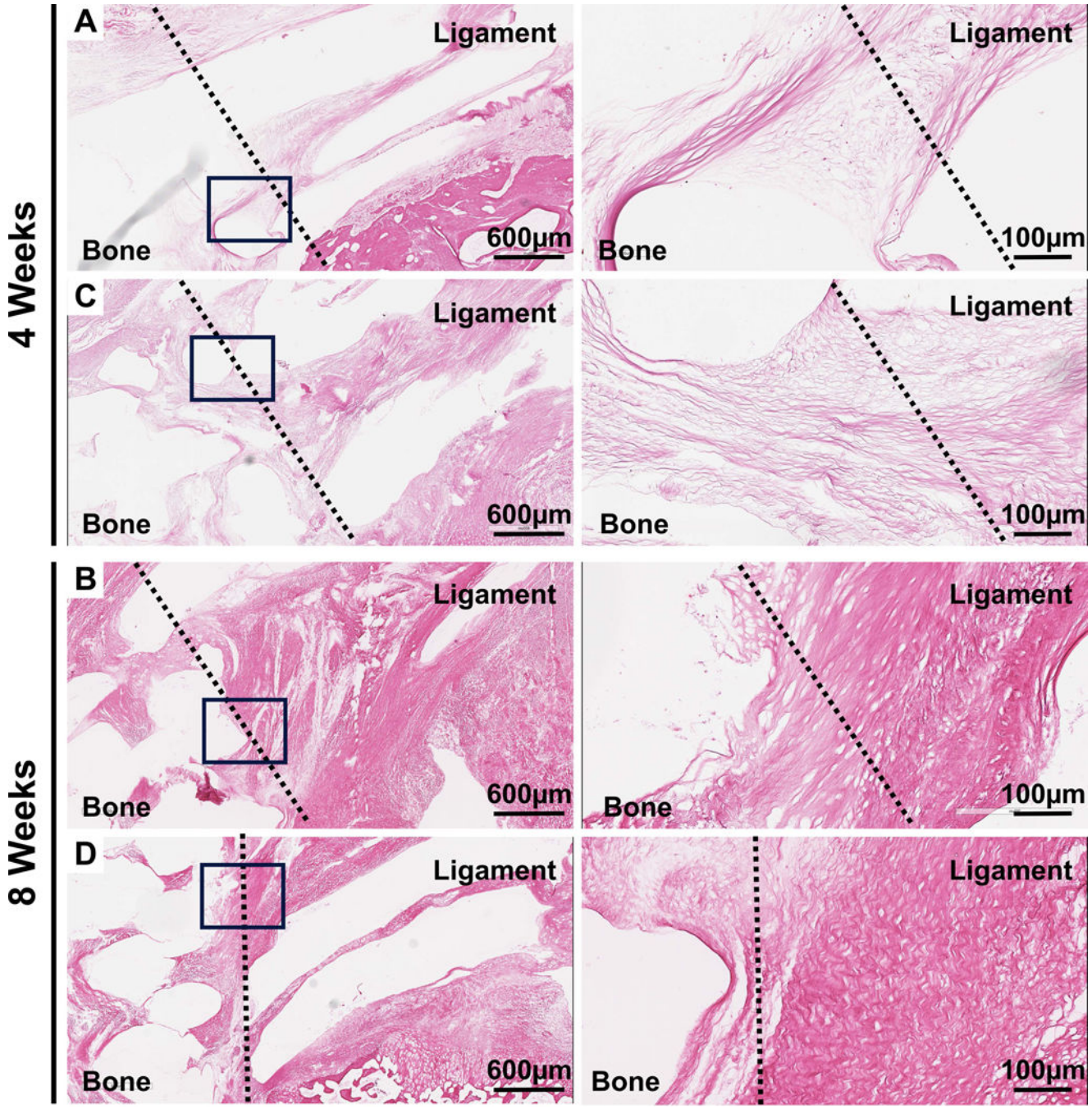

Figure 7:
H&E staining of the bone-ligament interface in samples implanted for 4 and 8 weeks. The solid boxes indicate the region of increased magnification in images on the right.

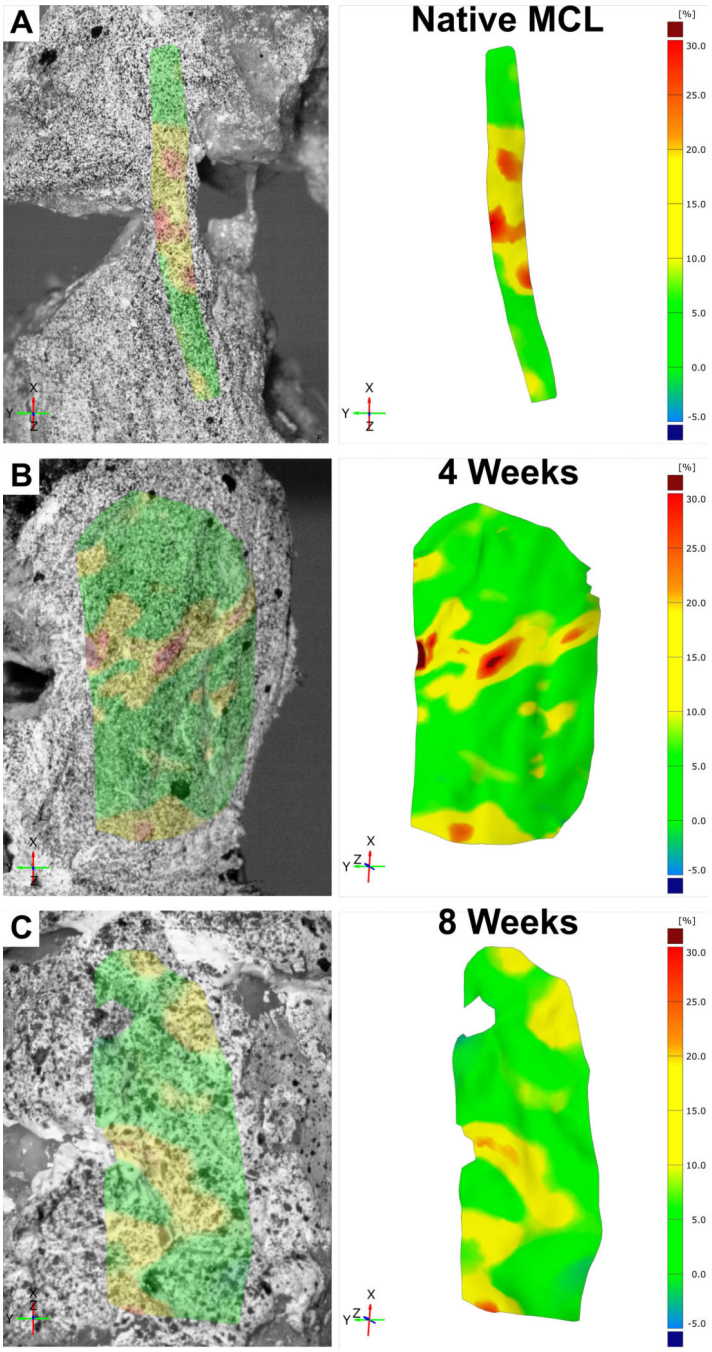

Figure 8:
Live strain maps of **A)** native MCL and multiphasic constructs at **B)** 4 weeks and **C)** 8 weeks post-implantation.

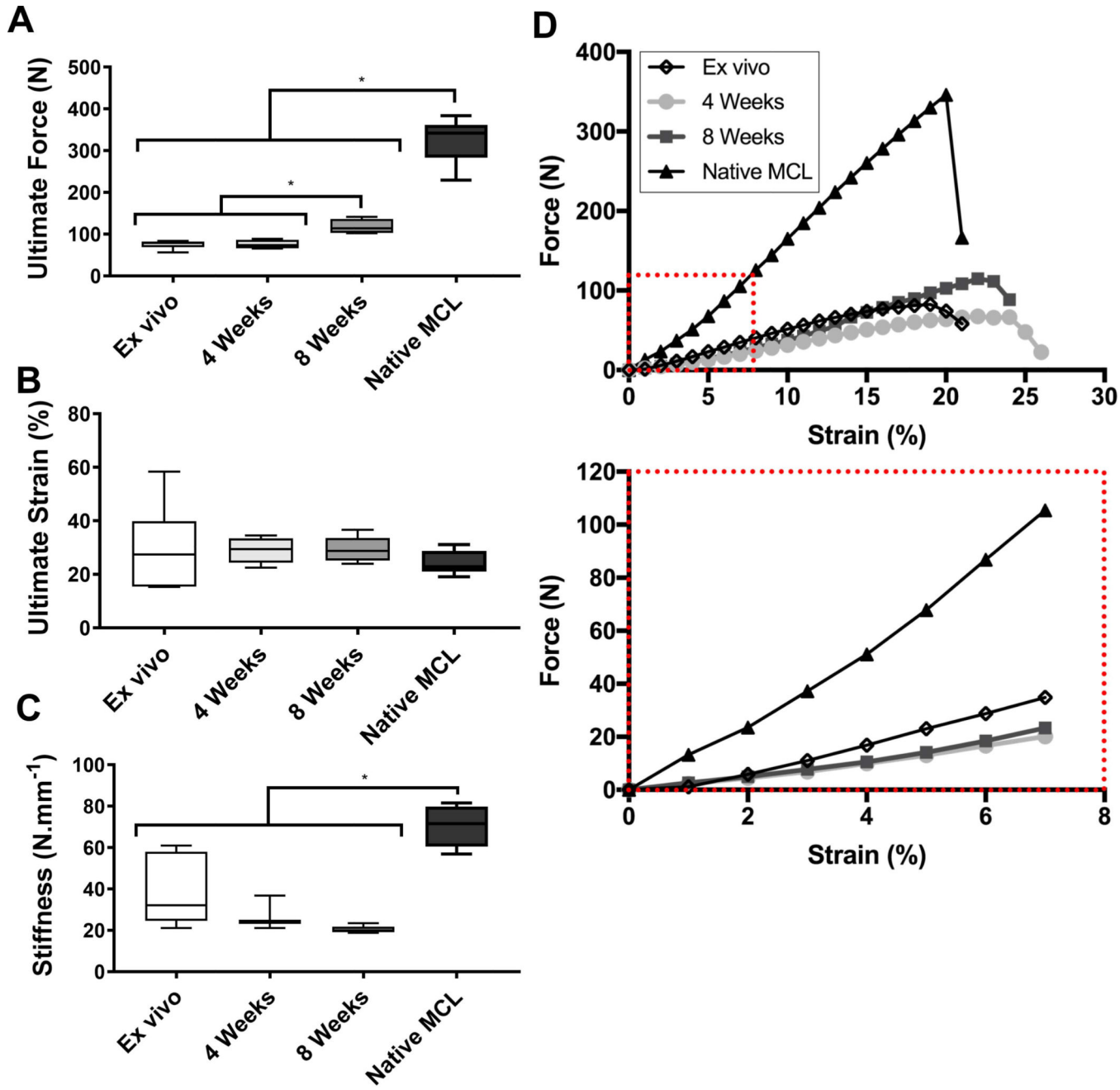

Figure 9:

Tensile testing results at elongation rate of 20mm/min. **A)** Ultimate force of ex vivo scaffolds, in vivo scaffolds and native MCL. **B)** Ultimate strain of ex vivo scaffolds, in vivo scaffolds and native MCL. **C)** Stiffness of ex vivo scaffolds, in vivo scaffolds and native MCL. **D)** Force Vs Strain displacement curves of ex vivo scaffolds, in vivo scaffolds and native MCL. Red box denotes zoomed in portion of Force Vs Strain displacement curves.

Table 1:

Tensile testing results of the 350μm scaffold in vivo at 4 and 8 weeks as compared to the ex vivo sample.

	Ex Vivo (n=5)	4W Ctrl (n=5)	8W Ctrl (n=5)	Native MCL (n=5)
Ultimate Force (N)	75±9	75±11	118±18	325±54
Ultimate Strain (%)	30±15	29±5	32±5	24±4
Stiffness (N/mm)	39±16	28±8	20±2	70±10
Failure Point	Mid-substance	Mid-substance	Mid-substance	Bone-ligament interface